

# Quantitative and multiplexed analysis of MMP-11 and CD45 in metastatic breast cancer tissues by immunohistochemistry-assisted LA-ICP-MS

Dylan Johnson<sup>1</sup>, David Clases<sup>1</sup>, Maria Luisa Fernández-Sánchez<sup>2</sup>, Noemí Eiró<sup>3</sup>, Luis O. González<sup>3</sup>, Francisco J. Vizoso<sup>3</sup>, Philip A. Doble<sup>1</sup>, Raquel González de Vega<sup>1\*</sup>

<sup>1</sup>The Atomic Medicine Initiative, University of Technology Sydney, NSW, Australia

<sup>2</sup>Department of Physical and Analytical Chemistry, University of Oviedo, Spain

<sup>3</sup>Research Unit, Hospital de Jove Foundation, Gijón, Spain

\*Corresponding author: email: Raquel.GonzalezdeVega@uts.edu.au

---

**ABSTRACT:** Breast cancer is the leading cause of cancer death and tremendous efforts are undertaken to limit dissemination and to provide effective treatment. Various histopathological parameters are routinely assessed in breast cancer to provide valuable predictive and prognostic information. MMP-11 and CD45 are tumour associated antigens and increasing evidence support the hypothesis that they are valuable biomarkers to interrogate tumours regarding aggressiveness and metastasis. This paper presents methods for quantitative and multiplexed imaging of MMP-11 and CD45 in breast cancer tissues and investigates their potential for improved cancer characterisation. An immunohistochemistry (IHC)-assisted LA-ICP-MS method was successfully developed and optimised using lanthanide tagged monoclonal antibodies as proxies for biomarker distributions and concentrations. The labelling degree of antibodies was determined via size exclusion – inductively coupled plasma – tandem mass spectrometry (SEC-ICP-MS/MS) employing on-line calibration via post-column isotope dilution analysis. To calibrate spatial intensity distributions of lanthanides in tissues, gelatine standards were spiked with element standards and analysed in parallel for external calibration. In conjunction with the determined labelling degree, this enabled the translation of lanthanide intensities into concentrations of biomarkers. A k-means clustering method was used to select tissue areas for statistical analysis and mean concentrations were compared for sets of metastatic, non-metastatic and healthy control samples. MMP-11 was expressed in stroma surrounding tumour areas, while CD45 was predominantly found inside tumour areas of high cell density. There was no significant correlation between CD45 and metastasis ( $p = 0.70$ ), however, MMP-11 was significantly upregulated (202%) in metastatic breast cancer compared to non-metastatic ( $p = 0.0077$ ) and control tissues ( $p = 0.0087$ ).

---

**Keywords** Element imaging · Immunoassays · Hyphenated techniques · SEC-ICP-MS · Biomarker quantification

## Introduction

Breast cancer is the leading cause of cancer death worldwide [1]. A key characteristic of breast cancer is its high capacity of invasion and metastasis which engenders an increased need for early detection and characterisation of breast tumours [2]. Tumour size, histological type, mitotic index, presence of necrosis, vascular invasion, as well as the status of hormonal receptors (ER and PR) and assessments of axillary lymph nodes are clinical parameters routinely investigated for diagnosis, treatment and prognosis of breast cancer [3]. However, these parameters may be extended by inclusion of recently discovered biomarkers that have the potential to provide complementary diagnostic and prognostic insights [4].

Matrix metalloproteinases (MMPs) belong to a family of zinc-dependent endopeptidases that contribute to tissue remodelling by degrading the extracellular matrix [5], which is a critical process in the carcinogenesis and metastasis of breast cancer tumours. The tumour microenvironment is composed of tumour cells, cytokines, and a variety of different non-tumour cells defined as tumour stromal cells including endothelial cells, fibroblasts, and inflammatory cells [6]. All of these components are linked in the tumour microenvironment and interact with each other dynamically. It has been discovered that the tumour microenvironment has a significant role in tumour formation and progression by transforming epithelial cells and changing their aptitude to give rise to malignant tumours [7,8].

Particularly, MMP-11 is a member of the stromelysin subgroup (stromelysin-3), which was first identified in stromal cells of breast carcinomas [9]. Studies have presented evidence that surrounding tumour cells and stromal cells express MMP-11 [10]. Kohrmann *et al.* assessed that MMP-11 as well as several other MMPs may be associated in breast cancer development and progression [11]. Specific receptors in breast cancer including oestrogen receptor (ER) and human epidermal growth factor receptor 2 (HER2) were found to be linked to MMP-11 expression in both tumours and stromal fibroblasts [12]. These findings suggest that MMP-11 is involved in certain signalling transduction pathways or unknown biological tumour behaviour, indicating a more complex role in cancer development than its proteolysis activity [6]. Min *et al.* demonstrated that MMP-11 expression was significantly related to clinicopathological parameters, which may be interrogated to predict disease outcome in patients with invasive ductal carcinoma, a type of breast cancer which accounts for 70-80% of breast cancer cases [12]. Furthermore, recent studies carried out by Gonzalez de Vega *et al.* [13,14] and Eiro *et al.* [15] showed that MMP-11 expression by stromal cells allows advanced classification and has potential as biomarker.

CD45 (PTPRC) is an enzyme of the protein tyrosine phosphatase (PTP) family. PTPs are signalling molecules that regulate a variety of cellular processes, including cell growth, differentiation, mitotic cycle, and oncogenic transformation. CD45 is a

type I transmembrane protein that is present in all differentiated hematopoietic cells [16]. It has been shown to be an essential regulator of T- and B-cell antigen receptor signalling. Caldwell and Patterson observed correlations between CD45 antigen, and the putative stages of cell differentiation for malignant B-cells at the earlier stages of malignancies, but found that a progressive loss of CD45 occurred at later stages [17]. Further research into the function of CD45 has indicated that interference in its regular processes may contribute to malignancy in breast cancer [18,19].

Routine clinical methods for breast cancer detection and classification are based on enzyme or fluorophore linked immunoassays, which enable visual interpretation by trained personal. However, these techniques are limited regarding the degree of multiplexing, sensitivity, and accuracy. Especially histopathological grading may be subject to discordance impacting accuracy and as such potentially treatment efficacy and prognosis [20]. A relatively new direction for biomarker analysis is elemental bio-imaging (EBI), which combines high sensitivity, linear dynamic range, unique quantification capabilities and robustness of inductively coupled plasma mass - spectrometry (ICP-MS) with the spatially resolved sampling of laser ablation (LA) to quantitatively assess elemental distributions in biological tissues [21]. It was previously shown that LA-ICP-MS may be employed to investigate the elemental content in tumours and their microenvironment and especially the possibility of making this technique popular for quantitative evaluations [22,23]. Quantification of elemental distribution is either possible by the parallel analysis of spiked standards or via on-line calibration techniques [24,25]. The implementation of immunohistochemical methods into the LA-ICP-MS workflow expanded the capabilities of this techniques beyond the sole analysis of elements and opened possibilities to target metal labels of antibodies as proxy for bio-indicative antigen/proteins.[21] As such, LA-ICP-MS is capable to perform analysis at the interface of metallomics and proteomics [26,27].

To increase sensitivity for high resolution or trace analysis, polymer tags offering binding sites for several isotopes have been established. The use of isotopically enriched elements became popular to increase the degree of multiplexing beyond to up to 40 [28]. The labelling process conjugates one or more polymer tags with variable size and number of isotopes to each antibody. As such, characterisation of the conjugate is required to determine labelling degrees and to perform reproducible workflows as well as quantitative analyses. This is possible by hyphenation of size exclusion chromatography (SEC) to ICP-MS(/MS) to separate and detect labelled antibodies. Post-column isotope dilution may simultaneously be used to determine absolute concentrations of both antibodies and labelled isotopes and to determine labelling degrees [25].

In this work, a quantitative multiplexed IHC method for LA-ICP-MS was developed and applied for quantitative and spatially resolved analysis of MMP-11 and CD45 in metastatic, non-metastatic and healthy control breast tissues. Comparisons across different samples supported the prognostic potential of MMP-11 in metastasis.

## Experimental

### Chemicals and consumables

High-purity ICP-MS standard calibration solutions of 10 mg L<sup>-1</sup> Nd, Eu and S were purchased from Choice Analytical (Thornleigh NSW, Australia). Enriched <sup>34</sup>S (91.24%) was obtained from ISC Science (Oviedo, Spain). The concentration of sulphur in this solution was determined by reverse isotope dilution analysis with a certified standard containing S with natural isotopic abundance. Ultra-pure water (18.2 MΩ cm) was obtained from a Sartorius 611 arium® pro water generation system (Sartorius Lab Instruments GmbH & Co. KG, Goettingen, Germany). Ammonium acetate (99.999% purity) was used to prepare the SEC eluent and was purchased from Sigma-Aldrich (Castle Hill, NSW, Australia).

Monoclonal anti-MMP11 (MAB3657) and anti-CD45 (MAB1430) antibodies were obtained from In-Vitro Technologies (VIC, Australia) and labelled with <sup>142</sup>Nd (97.95%) and <sup>170</sup>Er (96.92%), respectively, using the MAXPAR® antibody conjugation kits (Fluidigm; formerly DVS Sciences, San Francisco, CA) according to the manufacturer's standard protocol (version 4 06/13). Xylene and ethanol were obtained from ChemSupply (Gillman, SA, Australia). Bovine serum albumin (BSA), Triton X-100, normal goat serum (NGS), tris buffered saline (TBS) and phosphate buffered saline (PBS) were obtained from Sigma-Aldrich (Castle Hill, NSW, Australia).

### Sample collection

Paraffin-embedded human breast cancer and healthy breast samples were obtained from the Hospital de Jove Foundation (Gijón, Spain). The study adheres to national regulations and was approved by the Hospital de Jove Foundation Ethics and Investigation Committee (PI02/2018). H&E-stained tissue sections of all cancer samples were provided to locate and characterise the areas of interest within the tissue.

Additionally, colorimetric IHC standard staining of MMP-11, ER, PR and HER2 was performed in consecutive breast tissue sections following a protocol described by Eiró *et al.* [15] to determine the presence of these biomarkers within the tissue. Each sample was pathologically graded and awarded a score of 0 (negative) or 1 (positive). Clinicopathological characteristics of the breast tissue samples analysed in this study are listed in Table S1 of the Electronic Supplementary Material (ESM).

### Tissue staining procedure

Breast tissue samples were provided as formalin-fixed paraffin-embedded (FFPE) sections. Serial 5-µm sections were cut using a microtome (Leica Microsystems GmbH, Wetzlar, Germany) and transferred to adhesive-coated slides. Paraffin-embedded slides were first heated in a 60°C oven for 60-90 minutes. After baking, each slide was hydrated by incubation in the following solutions for five minutes, respectively: two xylenes solutions, 100% ethanol, 95% ethanol and 5% pure water, 50% ethanol and 50% pure water. Subsequently, slides were then kept in PBS (1x) until needed for staining.

For the main staining procedure, a hydrophobic border was drawn around the tissue, and a blocking solution comprising of 1% (w/v) BSA, 0.3% Triton X-100, 3% (v/v) NGS in PBS (1x) was applied for 45 minutes in a sealed environment mitigating unspecific binding of antibodies. The blocking solution was removed and the anti-CD45 antibody, diluted in a 1:50 mixture in blocking solution, was added onto the tissue section and incubated for two hours. Afterwards, the tissue was washed with

gentle agitation three times for five minutes in TBS (1x). Subsequently, the anti-MMP-11 antibody was applied in the same way at a 1:100 dilution. After antibody incubation, the tissue was washed and left to dry before storage and LA-ICP-MS analysis.

### Instrumentation

Antibody characterisation was carried out by SEC-ICP-MS/MS. SEC was performed using an ACQUITY UPLC Protein BEH SEC column with the dimensions 1.7  $\mu\text{m}$ , 2.1 x 150 mm (pore size 200  $\text{\AA}$ , MW range 10–450 kDa; Waters, Milford, MA, USA). The injection volume was 5  $\mu\text{L}$  and the flow rate was adjusted to 0.3  $\text{ml min}^{-1}$  using an Agilent 1200 Series HPLC System. The chromatographic system was coupled to an Agilent 8900 Triple Quadrupole ICP-MS/MS instrument (Agilent Technologies, Santa Clara, CA, USA). The instrument was operated in MS/MS mode using oxygen (99.995%, grade 4.5, North Ryde, NSW, Australia) as cell gas for mass shifting of sulphur. The performance of the ICP-MS instrument was tuned daily with a solution containing 1  $\mu\text{g L}^{-1}$  Li, Y, Tl and Ce to optimise sensitivity. The tune parameters for mass-shifting were optimised analysing a 200  $\text{ng g}^{-1}$  sulphur standard. The plasma was operated at 1.6 kW, oxygen was used as cell gas (18 %) and the typical nebuliser gas flow rate was 1.04  $\text{L min}^{-1}$ .

LA-ICP-MS experiments were performed with a New Wave Research NWR193 laser ablation system (New Wave Research, Fremont, CA, USA), coupled to an Agilent 7900 ICP-MS (Agilent Technologies, Santa Clara, CA, USA). The LA-ICP-MS was tuned for maximum sensitivity before each measurement using the reference material NIST 612 “Trace Elements in Glass”. Typical instrument parameters are outlined in Table 1. Images were analysed and created with the open source imaging software, *pew*<sup>2</sup> 1.2.1.[29]

H&E images were analysed with a ZEISS AxioScan Z.1 slide scanner (Carl Zeiss AG, Oberkochen, Germany).

### Antibody characterisation

Labelled antibodies were characterised by a double on-line isotope dilution SEC-ICP-MS method previously described by Clases *et al.* [25] A spike solution was continuously introduced (at 0.4  $\text{mL/min}$ ) through a T-piece. The spike solution contained a  $^{34}\text{S}$  isotope-enriched standard (200  $\text{ng g}^{-1}$ ), for IDA of the sulphur integral to the antibodies and standards of Nd and Er with natural isotopic abundances (1  $\mu\text{g g}^{-1}$ ) for reverse IDA of the isotopically enriched MAXPAR® labels. Experimental isotopic abundances of both spikes and samples were determined by off-line ICP-MS/MS to consider instrumental mass bias. The detector’s deadtime was determined and corrected by the analysis software (MassHunter, Agilent Technologies) analysing a diluted Er standard. Concentrations were obtained following the integration of the mass flow signals using R and RStudio and presented using OriginPro 2017 software (v8.0724, Microcal Software Inc., Northampton, MA, USA).

### Immunohistochemistry optimisations

To optimise contrasts, antibody titrations were performed using dilutions 1:100 and 1:500. In the cases of both anti-MMP-11 and anti-CD45, the 1:100 dilution provided improved contrast; however, high unspecific background staining was evident (Figure S1). This was corrected by decreasing the incubation period to 1 hour and by application of a thresholding algorithm to remove background levels from statistical analyses.

Multiplexing was achieved via sequential incubations of anti-MMP-11 and anti-CD45. The multiplexed method resulted in decreased staining of anti-CD45, as such, the dilution of anti-CD45 was finally adjusted to 1:50. The reproducibility of the multiplexed staining method was qualitatively assessed by staining and comparing three consecutive breast cancer tissue sections and LA-ICP-MS analyses produced comparable element distributions. Example figures depicting immunohistochemistry optimisation are provided in Figure S1. The application of dewaxing, washing and incubations steps corrupted the distribution of endogenous elements due to wash-out effects as well as contaminations (compare Figure S2). This pertained the simultaneous analysis and comparison of protein and endogenous element distributions.

### Calibration strategy

External calibration using mould-prepared gelatine standards was performed following the protocol previously described by Westerhausen *et al.* [24]. Calibration curves for Nd and Er were constructed by plotting the signal intensity obtained by LA-ICP-MS vs. the standards concentration (50, 100, 400, 700 and 1000  $\text{ng g}^{-1}$ ). The exact concentrations of the analytes in the standards were determined by digestion and liquid (off-line) ICP-MS analysis. The mean correlation coefficient of the calibration curves was 0.981 (RSD of 2.72%) across all measurements. Each data point for the subsequent analyses was then converted to concentration using linear regression on the calibration curve of the respective element.

### Statistical analysis

OriginPro 2017 was used to assess the significance of differences between factors with unpaired, two-tailed t-tests at a 95% confidence interval and equal variances not assumed.

*k*-means clustering, an algorithmic process which involves vectorisation of the data followed by calculation of *k* centroids, was

**Table 1.** Operating conditions for the ICP-MS and laser ablation system.

<b>Agilent 7900 ICP-MS</b>	
RF Power	1550 W
Nebuliser Gas	1.04 $\text{L min}^{-1}$
Isotopes	$^{142}\text{Nd}$ , $^{170}\text{Er}$ , $^{31}\text{P}$ , $^{13}\text{C}$ , $^{56}\text{Fe}$ , $^{63}\text{Cu}$ , $^{66}\text{Zn}$
Integration times	0.1 s (Nd, Er), 0.01 s (P, C, Fe, Cu, Zn)
<b>NWR193 LA System</b>	
Laser wavelength	193 nm
Fluence	20% (3 $\text{J/cm}^2$ )
Repetition rate	20 Hz
Spot size	35 $\mu\text{m}$
Scan speed	140 $\mu\text{m s}^{-1}$

used for image segmentation, and completed using functions of `pew2 1.2.1` [29,30].

## Results and Discussion

### Antibody characterisation and image thresholding

Determination of spatial protein concentrations in biological specimens by IHC-assisted LA-ICP-MS requires knowledge of the number of metal atoms labelled to the respective antibody. In this study, polymers loaded with isotopically enriched lanthanides were labelled to antibodies. The number of tags per antibody as well as the size and as such, the metal content of polymers is variable across different experiments and depends on nuanced preparation steps such as incubations times, ambient temperatures, humidity etc. Furthermore, knowledge of the exact labelled antibody concentration is required to enable repeatable staining and consequently contrasts. A protocol developed by Clases *et al.* [25] was applied to quantify the concentration of antibodies via the S content and the concentration of lanthanides in a double on-line IDA approach for SEC-ICP-MS/MS. The selective analysis of S required a mass shifting methods to mitigate the impact of polyatomic interferences such as  $^{16}\text{O}_2^+$ ,  $^{14}\text{N}^{18}\text{O}^+$ ,  $^{15}\text{N}^{17}\text{O}^+$ ,  $^{14}\text{N}^{17}\text{O}^+\text{H}^+$  [31]. Figure 1a demonstrates the SEC-ICP-MS/MS analysis of  $^{142}\text{Nd}$  labelled anti-MMP-11 and shows the transient signals of two S and Nd isotopes, respectively. S was quantified by addition of a  $^{34}\text{S}$  enriched post-column spike. As an isotopically enriched polymer tag was used to increase sensitivity, a naturally abundant Nd

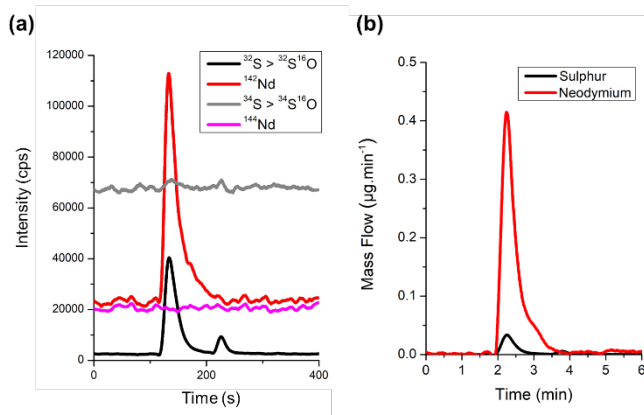


**Figure 1.** (a) Intensity chromatograms obtained by SEC-IDA-ICP-MS/MS analysis of  $^{142}\text{Nd}$  labelled anti-MMP-11. (b) Mass flow chromatogram of the same labelled antibody, calculated by isotope dilution analysis.

spike solution was added post-column for reverse on-line IDA. Figure 1b shows the S and Nd mass flow analysis which may be calculated from transient isotopes ratios. Integration provided the absolute mass of S and Nd in the injected volume and knowledge of the number of S atoms in the primary structure of the employed antibodies (IgG<sub>1</sub>: 32 S atoms, IgG<sub>2B</sub>: 36 S atoms for anti-CD45 and anti-MMP-11, respectively) enabled calculations of the molar labelling degree. In this study, labelling degrees for anti-MMP-11 and anti-CD45 were 104.0 and 112.2 (average number of lanthanide atoms per antibody). Furthermore, this technique determined the exact antibody concentration which was  $0.38 \text{ mg mL}^{-1}$  for anti-MMP-11 and  $0.65 \text{ mg}$

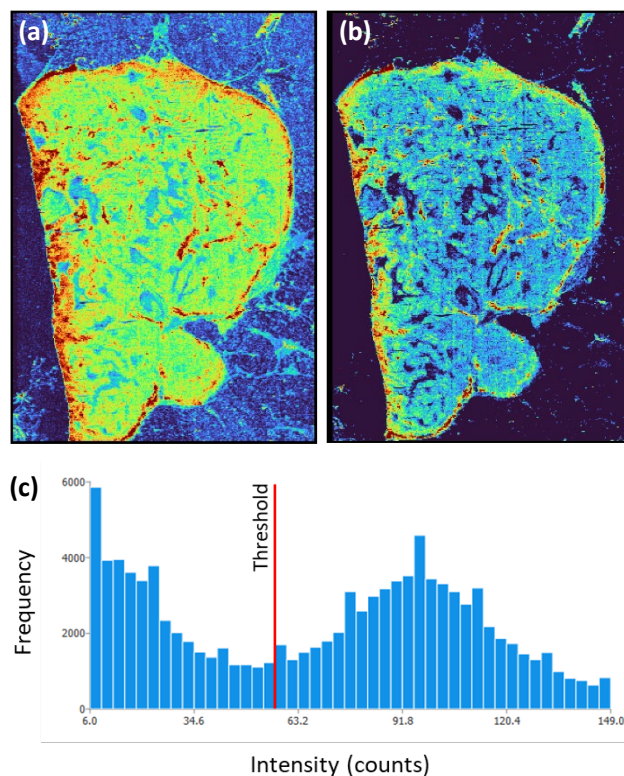


**Figure 2.** Example of background removal using ‘*k*-means clustering’ based segmentation on an LA-ICP-MS image. (a) Image before background removal, (b) image after background removal, (c) histogram visualisation of threshold.

$\text{mL}^{-1}$  for anti-CD45, these are relatively consistent with the approximate expected recovery of 60% for the MAXPAR® labelling process.

Characterised antibodies were subsequently used in IHC-protocols, analysed by LA-ICP-MS, and quantified via external calibration. The labelling degree was used to translate the lanthanide concentration into the corresponding antibody concentration. In this case, monoclonal antibodies which solely bind to one specific epitope of the targeted biomarkers were used and as such, the antibody mass concentrations were translated into the MMP-11 and CD45 concentration, respectively.

In quantitative image analysis, analysed regions outside of tissue areas or holes within the specimens lead to biased results and corresponding pixels must be removed prior to statistical analyses [32]. Common segmentation methods include, median, Otsu’s method, *k*-medians, and *k*-means enabling recognition and masking of non-tissue areas [33]. In this study a *k*-means clustering method ( $k = 3$ ) was employed to set a threshold under which a pixel was recognised as non-tissue area and masked as shown in Figure 2,  $k = 3$  was chosen based on the ‘elbow method’ described by Castellanos-Garcia *et al.* [30], and allows for segmentation between background, low concentration, and high concentration areas. Figure 2a shows the raw  $^{142}\text{Nd}$  intensity in a non-metastatic breast cancer tissue stained

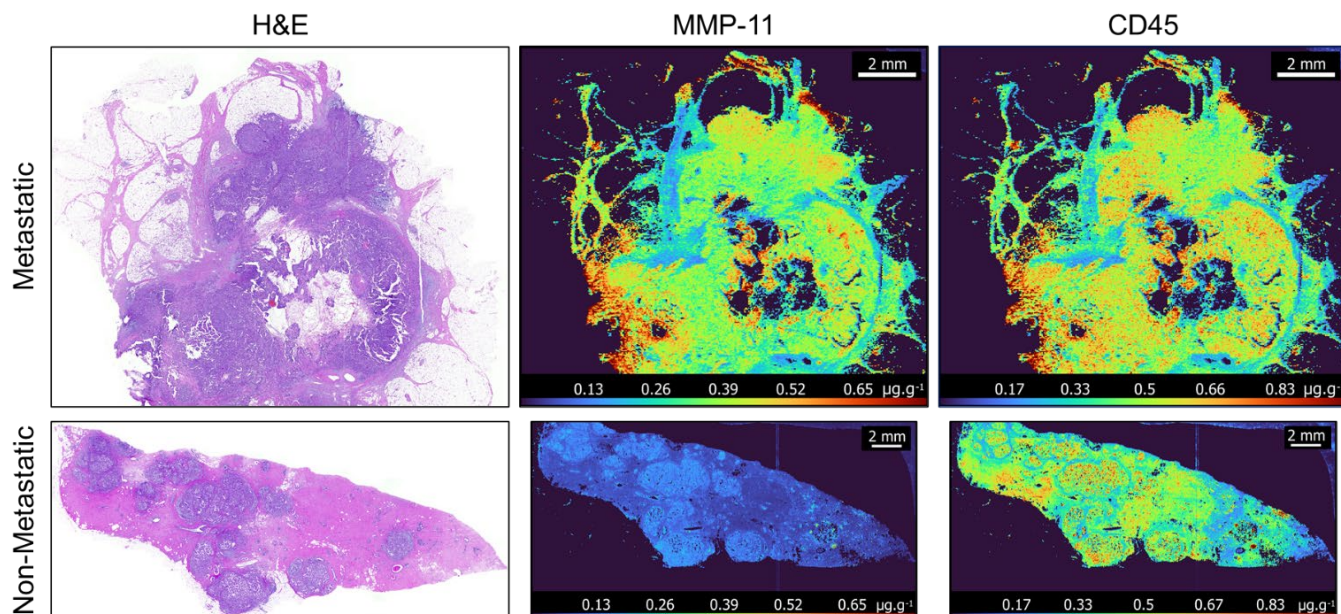


**Figure 3.** Exemplar images of metastatic (top) and non-metastatic (bottom) breast cancer tissue samples. **Left** - Images of H&E-stained consecutive tissue sections. **Centre** - Quantified LA-ICP-MS images of MMP-11 distribution. **Right** - Quantified LA-ICP-MS images of CD45 distribution. Background removed by *k*-means based thresholding.

with  $^{142}\text{Nd}$  labelled anti-MMP-11. While tissue areas and margins are clearly visible, it is obvious that ignoring unspecific background staining areas outside the tissue would lead to an inaccurate quantitative interpretation. Figure 2c shows the  $^{142}\text{Nd}$  intensity histogram of the image containing two signal populations. These populations correspond to unspecific background staining outside the tissue area (left) and the MMP-11 specific staining (right). In this example the *k*-means clustering threshold was determined to be 58 counts and pixels with intensities below this threshold were excluded from further analysis as displayed in Figure 2b.

#### Role of MMP11 and CD45 in breast cancer tissues

The characterised labelled antibodies were subsequently employed to investigate the quantitative spatial distribution of MMP-11 and CD45 in breast cancer tissues. Cu, Fe and Zn were acquired simultaneously to evaluate possible co-localisations with tumour areas. Distributions of Cu, Fe, and Zn distribution are shown in Figure S2. While there was an upregulation of these metals in tumour areas, there is no evidence of co-localisation with MMP-11 and CD45. However, it is likely that native element distributions were impacted by paraffination, deparaffinization and washing steps limiting both qualitative and quantitative analyses.

Spatially resolved concentrations of MMP-11 and CD45 were determined in metastatic ( $n = 12$ ), non-metastatic ( $n = 9$ ) and healthy breast tissue samples ( $n = 4$ ). Figure 3 shows the quantitative distribution of MMP-11 (centre) and CD45 (right) in one representative metastatic (top) and one representative non-metastatic samples (bottom). This example in figure 3 demonstrates that there was no notable link between metastasis and the expression of CD45, however, MMP-11 was significantly up-regulated in metastatic breast tissue. Furthermore, metastatic samples contained more heterogeneous distributions throughout the tumour microenvironment with concentrations values

reaching up to  $0.65 \mu\text{g g}^{-1}$  (see Figure 3 centre). This observation was consistent across the entire sample set and is in line with a previous study on the distribution of MMP-11 in a smaller cohort [14]. Comparison to the complementary H&E images allowed identification of different tissues and indicated that MMP-11 was overexpressed in stroma and tumour cells around the margins of large metastatic tumours. This is consistent with the role of MMP-11 as a factor involved in the degradation of the extracellular matrix. The MMP-11 distribution in non-metastatic breast cancer was more homogenous indicating that MMP-11 may have an important role in the metastatic process. CD45 was mostly localised in tumour areas with high cell densities and, unlike MMP-11, less in the adjacent stromal

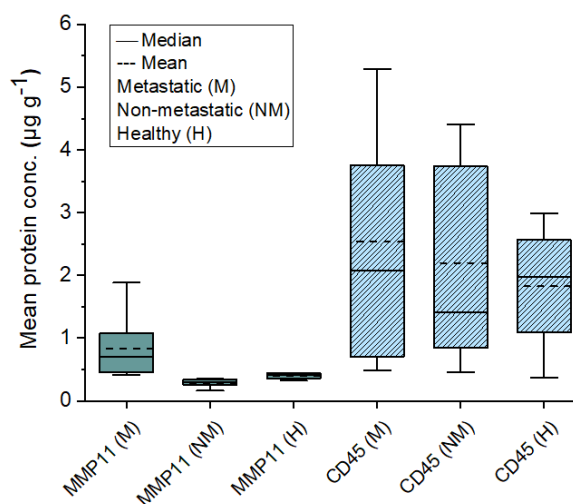


**Figure 4** Mean protein concentration of MMP-11 ( $n = 25$ ) and CD45 ( $n = 20$ ) obtained for metastatic, non-metastatic and healthy breast tissue sections.

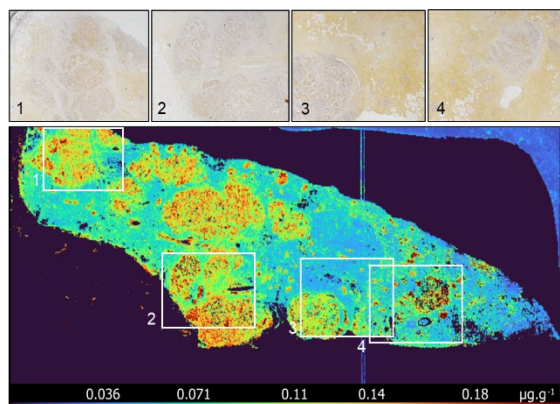


**Figure 5.** Visualisation of MMP11 in a non-metastatic breast cancer tissue by immunohistochemically-assisted LA-ICP-MS compared against traditional IHC staining.

areas. This is plausible as CD45 as a transmembrane protein was expected to be more abundant in areas of high cell density.

Across all samples, CD45 concentrations ranged from  $0.45 \pm 0.40 \mu\text{g g}^{-1}$  to  $5.28 \pm 1.43 \mu\text{g g}^{-1}$  and no significant differences between metastatic (mean:  $2.54 \pm 1.62 \mu\text{g g}^{-1}$ ) and non-metastatic (mean:  $2.20 \pm 1.60 \mu\text{g g}^{-1}$ ,  $p = 0.70$ ), or metastatic and healthy specimens (mean:  $1.83 \pm 0.95 \mu\text{g g}^{-1}$ ,  $p = 0.42$ ) were determined (compare Figure 4). However, MMP-11 was significantly increased by up to factor 3 (up to 202% increment) in metastatic tissues compared to non-metastatic ( $p = 0.0016$ ) and healthy tissues ( $p = 0.0077$ ). Healthy breast tissues analysed showed a significant increase of 43.5% compared to non-metastatic tissue for MMP-11 ( $p = 0.0087$ ). The mean concentration across all metastatic samples was  $0.74 \pm 0.41 \mu\text{g g}^{-1}$ , across non-metastatic samples  $0.25 \pm 0.06 \mu\text{g g}^{-1}$  and across tissues from healthy patients  $0.35 \pm 0.05 \mu\text{g g}^{-1}$ .

For further comparison routine colorimetric IHC testing were performed for MMP-11, PR, ER, and HER2 and graded as positive (1) or negative (0) to investigate correlations to concentrations of MMP-11 determined via IHC-assisted LA-ICP-MS (see Table S1). However, there was no significant link between PR, ER and HER2 gradings and concentrations of MMP-11 ( $p > 0.15$ ), which underpins the utility of MMP-11 as a prognostic factor providing complementary clinical data.

Additionally, in figure 5 the result of traditional IHC testing for MMP-11 was compared against the immunohistochemistry-assisted LA-ICP-MS method. The comparison shows a distribution which is consistent between both methods, with an advantage of the LA-ICP-MS method being a significant increase in sensitivity [34] allowing for more graduation and detailed analysis. Furthermore, quantitative analysis is useful for objective grading, alleviating concerns with visual grading, and providing important additional information to traditional IHC techniques.

## Conclusions

A multiplexed immunohistochemistry-assisted LA-ICP-MS method was developed to visualise and quantify the distribution of MMP-11 and CD45 in metastatic tumour tissues, non-metastatic tumour tissues and in control samples. Lanthanide polymer tags were conjugated to corresponding antibodies and to enable quantitative analysis, labelled antibodies were characterised by SEC-ICP-MS/MS using a double on-line IDA approach

to determine exact antibody concentrations and labelling degrees. A staining procedure was developed and raw intensities from labelled antibodies as proxy for the targeted biomarkers were calibrated using mould-prepared lanthanide spiked gelatine standards. Furthermore, *k*-means clustering algorithm was used to selectively investigate tissue areas while masking un-specific background staining.

CD45 was expressed in high cell density areas of tumours, however, no significant difference between metastatic, non-metastatic and control samples were found. On the other hand, MMP-11 was significantly overexpressed in the microenvironment of metastatic tumours tissues (mean:  $0.74 \pm 0.41 \mu\text{g g}^{-1}$ ) compared to both healthy (mean:  $0.35 \pm 0.05 \mu\text{g g}^{-1}$ ,  $p = 0.0016$ ) and non-metastatic tissue samples (mean:  $0.25 \pm 0.06 \mu\text{g g}^{-1}$ ,  $p = 0.0077$ ).

This study demonstrates the utility of IHC-assisted LA-ICP-MS as well as dedicated characterisation steps to accomplish quantitative imaging of bio-indicative proteins. The high sensitivity and resolution of LA-ICP-MS were specifically useful to probe the tumour microenvironment and to provide more nuanced data of protein expressions levels and for statistical models to objectively point out differences between various cohorts.

## Author Contributions

The manuscript was written through contributions of all authors. All authors have given approval to the final version of the manuscript.

## CRedit Author Statement

**Dylan Johnson:** Methodology, Validation, Formal analysis, Investigation, Writing - Original Draft **David Clases:** Conceptualisation, Methodology, Visualisation, Writing - Review & Editing **Maria Luisa Fernandez-Sanchez:** Conceptualisation, Writing - Review & Editing **Noemi Eiró:** Investigation, Writing - Review & Editing **Luis O. Gonzalez:** Investigation, Writing - Review & Editing **Francisco J. Vizoso:** Resources, Writing - Review & Editing **Philip A. Doble:** Resources, Writing - Review & Editing **Raquel Gonzalez de Vega:** Conceptualisation, Methodology, Investigation, Visualisation, Supervision, Writing - Review & Editing

## Acknowledgment

DJ is supported by an Australian Government Research Training Program Stipend. PAD is supported by Australian Research Council Discovery Project Grant (DP190102361).

The Agilent 7900 ICP-MS is a loan instrument provided by Agilent Australia for research use.

## Conflict of Interest

The authors declare no conflicts of interest.

## References

- [1] H. Sung, J. Ferlay, R.L. Siegel, M. Laversanne, I. Soerjomataram, A. Jemal, F. Bray, Global Cancer Statistics 2020: GLOBOCAN Estimates of Incidence and Mortality Worldwide for 36 Cancers in 185 Countries,

- CA Cancer J Clin. 71 (2021) 209–249. <https://doi.org/10.3322/caac.21660>.
- [2] C. DeSantis, J. Ma, L. Bryan, A. Jemal, Breast cancer statistics, 2013, CA: A Cancer Journal for Clinicians. 64 (2014) 52–62. <https://doi.org/10.3322/caac.21203>.
- [3] E. Mallon, P. Osin, N. Nasiri, I. Blain, B. Howard, B. Gusterson, The Basic Pathology of Human Breast Cancer, Journal of Mammary Gland Biology and Neoplasia. 5 (2000) 139–163. <https://doi.org/10.1023/a:1026439204849>.
- [4] N. Patani, L.-A. Martin, M. Dowsett, Biomarkers for the clinical management of breast cancer: International perspective: Biomarkers of breast cancer, Int. J. Cancer. 133 (2013) 1–13. <https://doi.org/10.1002/ijc.27997>.
- [5] B. Davidson, R. Reich, B. Risberg, J.M. Nesland, The biological role and regulation of matrix metalloproteinases (MMP) in cancer, Arkh Patol. 64 (2002) 47–53.
- [6] X. Zhang, S. Huang, J. Guo, L. Zhou, L. You, T. Zhang, Y. Zhao, Insights into the distinct roles of MMP-11 in tumor biology and future therapeutics (Review), Int. J. Oncol. 48 (2016) 1783–1793. <https://doi.org/10.3892/ijo.2016.3400>.
- [7] Matrix metalloproteinase stromelysin-3 in development and pathogenesis, Histology and Histopathology. (2005) 177–185. <https://doi.org/10.14670/HH-20.177>.
- [8] S. Frisch, H. Francis, Disruption of epithelial cell-matrix interactions induces apoptosis, The Journal of Cell Biology. 124 (1994) 619–626. <https://doi.org/10.1083/jcb.124.4.619>.
- [9] P. Basset, J.P. Bellocq, C. Wolf, I. Stoll, P. Hutin, J.M. Limacher, O.L. Podhajcer, M.P. Chenard, M.C. Rio, P. Chambon, A novel metalloproteinase gene specifically expressed in stromal cells of breast carcinomas, Nature. 348 (1990) 699–704. <https://doi.org/10.1038/348699a0>.
- [10] J.I. Barrasa, N. Olmo, A. Santiago-Gómez, E. Lecona, P. Anglard, J. Turnay, M.A. Lizarbe, Histone deacetylase inhibitors upregulate MMP11 gene expression through Sp1/Smad complexes in human colon adenocarcinoma cells, Biochimica et Biophysica Acta (BBA) - Molecular Cell Research. 1823 (2012) 570–581. <https://doi.org/10.1016/j.bbamcr.2011.12.010>.
- [11] A. Köhrmann, U. Kammerer, M. Kapp, J. Dietl, J. Anacker, Expression of matrix metalloproteinases (MMPs) in primary human breast cancer and breast cancer cell lines: New findings and review of the literature, BMC Cancer. 9 (2009) 188. <https://doi.org/10.1186/1471-2407-9-188>.
- [12] K.-W. Min, D.-H. Kim, S.-I. Do, J.-S. Pyo, K. Kim, S.W. Chae, J.H. Sohn, Y.-H. Oh, H.J. Kim, S.H. Choi, Y.J. Choi, C.H. Park, Diagnostic and Prognostic Relevance of MMP-11 Expression in the Stromal Fibroblast-Like Cells Adjacent to Invasive Ductal Carcinoma of the Breast, Ann Surg Oncol. 20 (2013) 433–442. <https://doi.org/10.1245/s10434-012-2734-3>.
- [13] R. González de Vega, M.L.F. Sanchez, N. Eiro, F.J. Vizoso, M. Sperling, U. Karst, A.S. Medel, Multimodal laser ablation/desorption imaging analysis of Zn and MMP-11 in breast tissues, Anal Bioanal Chem. 410 (2018) 913–922. <https://doi.org/10.1007/s00216-017-0537-x>.
- [14] R. González de Vega, D. Clases, M.L. Fernández-Sánchez, N. Eiró, L.O. González, F.J. Vizoso, P.A. Doble, A. Sanz-Medel, MMP-11 as a biomarker for metastatic breast cancer by immunohistochemical-assisted imaging mass spectrometry, Anal Bioanal Chem. 411 (2019) 639–646. <https://doi.org/10.1007/s00216-018-1365-3>.
- [15] N. Eiro, S. Cid, B. Fernández, M. Fraile, A. Cernea, R. Sánchez, A. Andicoechea, E.J.D. Galiana, L.O. González, Z. Fernández-Muñiz, J.L. Fernández-Martínez, F.J. Vizoso, MMP11 expression in intratumoral inflammatory cells in breast cancer, Histopathology. 75 (2019) 916–930. <https://doi.org/10.1111/his.13956>.
- [16] N. Holmes, CD45: all is not yet crystal clear, Immunology. 117 (2006) 145–155. <https://doi.org/10.1111/j.1365-2567.2005.02265.x>.
- [17] C.W. Caldwell, W.P. Patterson, Relationship between CD45 antigen expression and putative stages of differentiation in B-cell malignancies, Am. J. Hematol. 36 (1991) 111–115. <https://doi.org/10.1002/ajh.2830360209>.
- [18] B. Ruffell, A. Au, H.S. Rugo, L.J. Esserman, E.S. Hwang, L.M. Coussens, Leukocyte composition of human breast cancer, PNAS. 109 (2012) 2796–2801. <https://doi.org/10.1073/pnas.1104303108>.
- [19] M.L. Hermiston, Z. Xu, A. Weiss, CD45: A Critical Regulator of Signaling Thresholds in Immune Cells, Annual Review of Immunology. 21 (2003) 107–137. <http://dx.doi.org.ezproxy.lib.uts.edu.au/10.1146/annurev.immunol.21.120601.140946>.
- [20] R.A. Walker, Quantification of immunohistochemistry issues concerning methods, utility and semiquantitative assessment I, Histopathology. 49 (2006) 406–410. <https://doi.org/10.1111/j.1365-2559.2006.02514.x>.
- [21] P.A. Doble, R.G. de Vega, D.P. Bishop, D.J. Hare, D. Clases, Laser Ablation-Inductively Coupled Plasma-Mass Spectrometry Imaging in Biology, Chem. Rev. (2021). <https://doi.org/10.1021/acs.chemrev.0c01219>.
- [22] D. P. Bishop, D. Clases, F. Fryer, E. Williams, S. Wilkins, D. J. Hare, N. Cole, U. Karst, P. A. Doble, Elemental bio-imaging using laser ablation-triple quadrupole-ICP-MS, Journal of Analytical Atomic Spectrometry. 31 (2016) 197–202. <https://doi.org/10.1039/C5JA00293A>.
- [23] R.G. de Vega, M.L. Fernández-Sánchez, J. Pisonero, N. Eiró, F.J. Vizoso, A. Sanz-Medel, Quantitative bioimaging of Ca, Fe, Cu and Zn in breast cancer tissues by LA-ICP-MS, J. Anal. At. Spectrom. 32 (2017) 671–677. <https://doi.org/10.1039/C6JA00390G>.
- [24] M.T. Westerhausen, T.E. Lockwood, R. Gonzalez de Vega, A. Röhnelt, D.P. Bishop, N. Cole, P.A. Doble, D. Clases, Low background mould-prepared gelatine standards for reproducible quantification in elemental bio-imaging, Analyst. 144 (2019) 6881–6888. <https://doi.org/10.1039/C9AN01580A>.
- [25] D. Clases, R.G. de Vega, P.A. Adlard, P.A. Doble, Online reverse isotope dilution analysis for spatial quantification of elemental labels used in immunohistochemical assisted imaging mass spectrometry via LA-ICP-MS, J. Anal. At. Spectrom. 34 (2019) 407–412. <https://doi.org/10.1039/C8JA00324F>.
- [26] B. Paul, D.J. Hare, D.P. Bishop, C. Paton, V.T. Nguyen, N. Cole, M.M. Niedwiecki, E. Andreozzi, A. Vais, J.L. Billings, L. Bray, A.I. Bush, G. McColl, B.R. Roberts, P.A. Adlard, D.I. Finkelstein, J. Hellstrom, J.M. Hergt,

- J.D. Woodhead, P.A. Doble, Visualising mouse neuroanatomy and function by metal distribution using laser ablation-inductively coupled plasma-mass spectrometry imaging, *Chem. Sci.* 6 (2015) 5383–5393. <https://doi.org/10.1039/C5SC02231B>.
- [27] D. Clases, R. Gonzalez de Vega, S. Funke, T.E. Lockwood, M.T. Westerhausen, R.V. Taudte, P.A. Adlard, P.A. Doble, Matching sensitivity to abundance: high resolution immuno-mass spectrometry imaging of lanthanide labels and endogenous elements in the murine brain, *J. Anal. At. Spectrom.* 35 (2020) 728–735. <https://doi.org/10.1039/C9JA00405J>.
- [28] M.E. Ijsselsteijn, R. van der Breggen, A. Farina Sarasqueta, F. Koning, N.F.C.C. de Miranda, A 40-Marker Panel for High Dimensional Characterization of Cancer Immune Microenvironments by Imaging Mass Cytometry, *Frontiers in Immunology*. 10 (2019) 2534. <https://doi.org/10.3389/fimmu.2019.02534>.
- [29] T.E. Lockwood, M.T. Westerhausen, P.A. Doble, Pew2: Open-Source Imaging Software for Laser Ablation–Inductively Coupled Plasma–Mass Spectrometry, *Anal. Chem.* (2021). <https://doi.org/10.1021/acs.anal-chem.1c02138>.
- [30] L.J. Castellanos-García, S.G. Elci, R.W. Vachet, Reconstruction, analysis, and segmentation of LA-ICP-MS imaging data using Python for the identification of sub-organ regions in tissues, *Analyst*. 145 (2020) 3705–3712. <https://doi.org/10.1039/C9AN02472G>.
- [31] T.W. May, R.H. Wiedmeyer, A table of polyatomic interferences in ICP-MS, *ATOMIC SPECTROSCOPY*. 19 (1998) 150–155.
- [32] M.M. Niedzwiecki, C. Austin, R. Remark, M. Merad, S. Gnjjatic, G. Estrada-Gutierrez, A. Espejel-Nuñez, H. Borboa-Olivares, M. Guzman-Huerta, R.J. Wright, R.O. Wright, M. Arora, A multimodal imaging workflow to visualize metal mixtures in the human placenta and explore colocalization with biological response markers†, *Metalomics*. 8 (2016) 444–452. <https://doi.org/10.1039/c6mt00010j>.
- [33] D.P. Bishop, M.T. Westerhausen, F. Barthelemy, T. Lockwood, N. Cole, E.M. Gibbs, R.H. Crosbie, S.F. Nelson, M.C. Miceli, P.A. Doble, J. Wanagat, Quantitative immuno-mass spectrometry imaging of skeletal muscle dystrophin, *Sci Rep*. 11 (2021) 1128. <https://doi.org/10.1038/s41598-020-80495-8>.
- [34] R.M. Levenson, A.D. Borowsky, M. Angelo, Immunohistochemistry and mass spectrometry for highly multiplexed cellular molecular imaging, *Lab Invest*. 95 (2015) 397–405. <https://doi.org/10.1038/labinvest.2015.2>.